Journal of the Geological Society, London, Vol. **156**, 1999, pp. 247–259. Printed in Great Britain

The Palaeoproterozoic Tchilit exotic terrane (Aïr, Niger) within the Pan-African collage of the Tuareg shield

J. NAVEZ[1], J. P. LIÉGEOIS[1], L. LATOUCHE[2], A. BOVEN[3] & R. BLACK[2]

[1]*Département de Géologie, Musée Royal de l'Afrique Centrale, B-3080 Tervuren, Belgium (e-mail: jplieg@rulb.ac.be)*

[2]*CNRS, ESA7058, Laboratoire de Minéralogie, Muséum National d'Histoire Naturelle, 61 rue Buffon, F-75005 Paris, France*

[3]*Eenheid Geochronologie, Vrije Universiteit Brussel, Pleinlaan 2, B-1050 Brussel, Belgium*

Abstract: The Tchilit terrane in Aïr (Niger) is one of the most exotic terranes among those constituting the Tuareg shield. It is composed of low-K calc-alkaline metabasalts and meta-andesites (amphibolites), alkaline metarhyolites, detrital metasediments and of a syenogranite. Volcanic protoliths are Palaeoproterozoic in age (within the 1600–2200 Ma time span; Sm–Nd, Rb–Sr and Ar–Ar systematics) and underwent two metamorphisms accompanied by mylonitization. The first, amphibolite-facies (690 ± 40°C) metamorphism occurred during the Palaeoproterozoic whereas the second is a greenschist retrogression, late Pan-African in age (646 ± 6 Ma, 2σ, Ar–Ar age). The metasediments have been affected only by the Pan-African event and are probably Neoproterozoic. The syenogranite (619 ± 39 Ma, 2σ, Rb–Sr) is later than both metamorphisms: it is the only Pan-African material in Tchilit. The Pan-African tectonics, a N–S transpression (dextral shear) induced the overthrusting of the neighbouring Assodé terrane onto Tchilit. Major, trace elements and Sr–Nd isotopes give to the protoliths of amphibolites a continental active margin signature (low-K calc-alkaline) and to those of the metarhyolites an alkaline one, more typical of a post-collisional or intraplate setting. Both were significantly contaminated by an early Archaean crust (Sm–Nd T_{DM} model ages >3 Ga). Whether these two magmatisms were generated in the same environment or not is unresolved. In any case, the Tchilit terrane is distinctive from the 2.1 Ga Birimian volcanosedimentary series of the West African craton that are entirely juvenile. Tchilit is the first Palaeoproterozoic non-granulitic terrane found in the Pan-African assembly of the Tuareg shield which raises questions about its provenance.

Keywords: Tuareg shield, Pan-African orogeny, volcanism, geochemistry, geochronology.

Recently, the Tuareg shield, part of the Trans-Saharan belt, has been reinterpreted as a collage of terranes (Fig. 1; Black *et al.* 1994) that was assembled in a two-stage Neoproterozoic Pan-African Orogeny (750–660 Ma and 650–550 Ma; Liégeois *et al.* 1994). In the Aïr region (southeastern Tuareg shield; 60 000 km^2; Fig. 1), the sequence of events leading to the amalgamation of the three major terranes (Assodé, Barghot and Aouzegueur) fits into a coherent palaeogeodynamic setting (Liégeois *et al.* 1994). A fourth 'suspect' terrane, Tchilit, cropping out in a small area (350 km^2) at the southwestern tip of the Aïr, was not integrated in the model because of lack of lithological, metamorphic or magmatic correlations. Present additional geochemical, isotopic and petrological data confirm the origin of the Tchilit terrane which contains well-preserved pre-Pan-African metamorphic assemblages. Tchilit appears thus as exotic relative to the three other Aïr terranes, entirely fashioned by the Pan-African orogeny. The preservation of pre-Pan-African features in the Tchilit terrane throws light on the palaeogeodynamic environments that prevailed prior to the Pan-African Orogeny.

Assembly of terranes in the Tuareg shield, with special reference to Aïr

The Tuareg shield formed during the Pan-African Orogeny (750–550 Ma) and is made up of 23 identified terranes most often separated by N–S mega-shear zones, but also by major thrusts (Fig. 1; Black *et al.* 1994). The origin of this structure is best understood in Aïr (Fig. 2; Liégeois *et al.* 1994) whose Pan-African evolution can be summarized as follows.

(1) *Early Pan-African event.* Westward subduction of an eastern oceanic domain generated an island arc and a back-arc basin (ophiolite) whose remnants are now found in Aouzegueur (Fig. 2), the most easterly terrane in Aïr. Relics of this period such as arc continental margin metabasalts, also exist in the Barghot terrane but in minor amounts (work in progress). In the third more westerly terrane, Assodé (Fig. 2), no evidence of this arc stage has been observed so far. Subsequent collision induced high temperature/high pressure metamorphism and is responsible for the thrusting of the two eastern terranes (Barghot and Aouzegueur) onto the eastern cratonic passive margin (inferred East Saharan 'ghost' craton; Black & Liégeois 1993). This was accompanied by the intrusion of medium-K (Aouzegueur) and high-K (Barghot) calc-alkaline granitoids (730–664 Ma, U–Pb zircon; Liégeois *et al.* 1994). In contrast, the Assodé terrane, which strongly collided with the East Saharan craton, underwent a high-temperature–low-pressure metamorphism and was invaded by a regional anatectic potassic leucogranite of lower crustal origin (Renati granite, 666 ± 11 Ma, Rb–Sr) in a context of lithospheric mantle delamination following thickening (Black & Liégeois 1993; Liégeois *et al.* 1994). At this period, Tchilit was probably not involved in the collision since it has not recorded any event in that age range.

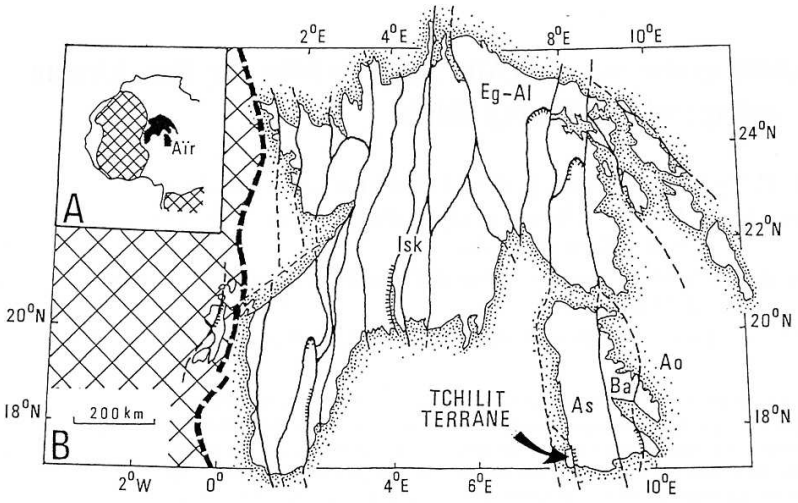

Fig. 1. (**a**) West Africa with Aïr location; black: Tuareg shield; criss-cross: West African craton. (**b**) Map of the Tuareg shield assembly of terranes (modified after Black *et al.* 1994). Terranes cited in the text: As, Assodé; Ao, Aouzegueur; Ba, Barghot; Eg-Al, Egéré–Aleksod; Isk, Iskel. Criss-cross: West African craton, heavy dashed line: Pan-African main suture; heavy lines: main shear zones (dashed when inferred); barbed lines: mains thrusts. The two latter structures are terrane boundaries.

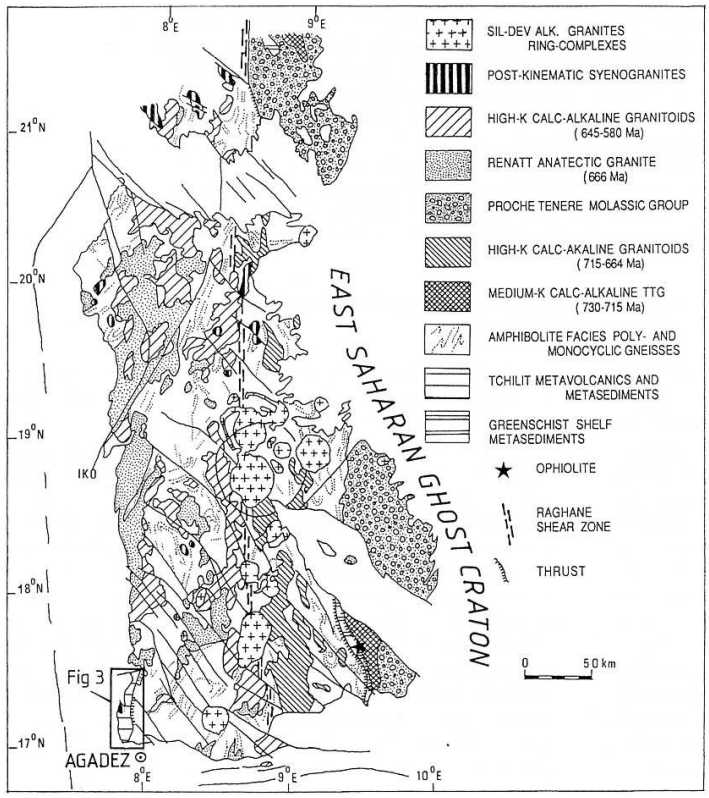

Fig. 2. Simplified geological map of the Aïr region (modified after Liégeois *et al.* 1994), including the Tchilit terrane.

(2) *Late Pan-African event*. The Barghot and Aouzegueur thrust terranes were protected by the underlying rigid East Saharan craton and escaped most of this phase. The Assodé terrane, located to the west, was invaded by large N–S-elongated high-K calc-alkaline batholiths (645–580 Ma, U–Pb zircon and Rb–Sr; Liégeois *et al.* 1994) and affected by a second less intense high-temperature metamorphism. This phase is related, in a post-collisional setting, to an easterly dipping subduction zone located to the west of the Assodé terrane with an oblique ridge–trench disposition, responsible for the displacement of Assodé by an estimated distance of 1000 km to the north. This movement is best recorded in the N–S Raghane shear zone with a mean width of 5 km marked by amphibolite-facies mylonites. Raghane is cut by a stitch granite dated at 580 Ma (U–Pb zircon, Bertrand *et al.* 1978). The lithospheric scale of this mega-shear zone is attested by the

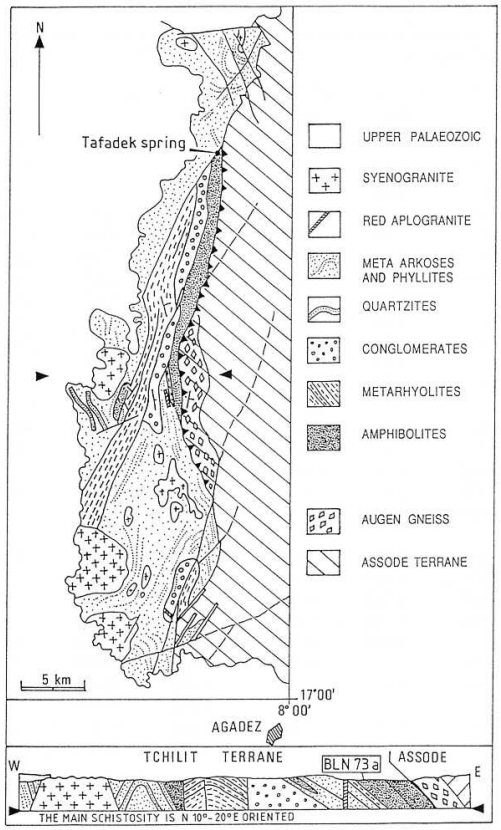

Fig. 3. Simplified geological map and cross-section of the Tchilit terrane.

intrusion along it of alkaline ring-complexes with anorthosites of mantle origin, around 410 Ma (Rb–Sr, Moreau *et al.* 1994).

This model (see Liégeois *et al.* 1994 for details) is the basis for the new interpretation of the Tuareg shield in terms of a collage of terranes. It is likely, as in the case of the Aïr, that most of the Tuareg terranes were displaced within a single, although complex, palaeogeodynamic environment. However, some terranes are quite exotic exhibiting very special characteristics. Black *et al.* (1994) noted the unique 870–840 Ma time interval for syn- to late-kinematic granitoids (Caby *et al.* 1982) in the Iskel terrane (Fig. 1). The Tchilit terrane with its peculiar lithologies, metamorphism and isotopic characteristics also constitutes an exotic block within the displaced terranes of the eastern Tuareg shield.

The Tchilit exotic terrane

To the west, subhorizontal Upper Palaeozoic sediments unconformably overlie the Tchilit block. To the east, the contact between the Tchilit and the Assodé terrane is a steep thrust with a westerly vergence (Fig. 3). The associated stretching lineations pitch 5° to 10° on a N20° direction. This thrust has transformed a high-K calc-alkaline granite of Assodé (640–580 Ma) into augen gneiss and has to be considered as a late event. The overriding of Assodé onto Tchilit is a consequence of dextral N–S movements induced by transpression. In Assodé, however, these structures are local and have only affected the western margin of this terrane, which, at this moment, behaved as a relatively rigid body.

In the Tchilit block, four main lithologies were differentiated by Black *et al.* (1967): amphibolites, metarhyolites, often delimited by NNE-striking faults, greenschist detrital metasediments, and intrusive syenogranites (Fig. 3).

The amphibolites are particularly well developed along the eastern margin of the terrane where they form a kilometre-wide strip. They are generally very fine-grained, can be massive or may display a schistosity and a stretching lineation parallel to that of the overlying mylonitic augen gneiss of Assodé. Another effect of mylonitization is the occurrence of massive amphibolites as boudins within amphibolite schists and detrital metasediments.

The metarhyolites are fine-grained and brown to black in colour. Although mostly mylonitic, they appear massive in the field, displaying a primary schistosity underlined by biotite and K-feldspar porphyroclasts. In these metarhyolites, some thin levels show vesuvianite porphyroblasts with plagioclase and quartz.

The detrital metasediments comprise fine-grained quartzites and arkoses, a well-sorted quartz-pebble conglomerate, purplish muscovite phyllites and poorly sorted conglomerates containing cobbles of pink granite, amphibolites and other rocks set in a quartz–feldspar matrix. In arkosic and quartzitic horizons, the schistosity is underlined by muscovite. These rocks have been affected by only a single metamorphic event in greenschist facies. Their contacts with the metavolcanic rocks were transposed by this greenschist mylonitization.

The biotite perthite syenogranite is medium- to coarse-grained, pink in colour, displays a hypidiomorphic structure without deformation and develops a fine-grained marginal facies where it is cut by aplite veins. Locally, it contains xenoliths of the country rocks (purplish muscovite phyllites) and was seen net-veining the metarhyolites. Many bodies of such a granite, 50 m to 5 km in diameter occur in the Tchilit terrane. Brick-red aplogranite dykes have frequently been injected along the NNE-striking faults.

Pressure–temperature conditions

The amphibolites, despite their fine-grained texture, display a primary metamorphic paragenesis with hornblende, plagioclase and ilmenite. Relict diopside is present in some samples. For the basaltic compositions, amphibole–plagioclase thermometry (Holland & Blundy 1994) indicates temperatures within the range 690 ± 40°C at 5 kbar (Table 1).

In the metarhyolite sequence, comprising Ca–Fe rich intercalated horizons and mylonitic metarhyolites, the parageneses vesuvianite–plagioclase–quartz (Fig. 4a) and K-feldspar–biotite–quartz (Fig. 4b) yield^{s} temperature estimate of 720 ± 30°C (Table 1), a similar temperature interval within error limits as for the amphibolites. This points to a unique amphibolite-facies metamorphism at *c.* 700°C having affected both metarhyolites and amphibolites.

Secondary Pan-African deformation and metamorphic retrogression are concentrated along shear planes with the development of epidote and chlorite in the amphibolites, and chlorite and muscovite in the metarhyolites as well as in the quartzites, meta-arkoses, phyllites and conglomerates. This corresponds to the mylonitization of the augen gneiss of the Assodé overriding margin.

Table 1. *Representative microprobe mineral analyses used in thermometry*

	Amphiboles			Cpx	Plagioclase				Vesuvianite		
No. analysis	BLN277 d/60	BLN282 1/4	BLN282 2/5	BLN282 1/2	BLN282 1/8	BLN282 1/18	BLN277 b/43	BLN277 b/44	BLN277 b/34	BLN277 b/36	BLN277 b/37
SiO_2	45.22	44.14	46.93	51.87	55.68	56.62	60.78	60.47	36.71	36.81	36.33
TiO_2	0.24	0.49	0.41	0.16	0.00	0.07	0.01	0.00	1.29	0.99	0.69
Al_2O_3	8.17	10.70	8.29	0.84	27.99	28.16	25.18	24.93	8.80	9.04	10.11
Cr_2O_3	0.06	0.10	0.10	0.12	0.00	0.03	0.00	0.00	0.09	0.00	0.15
NiO	0.00	0.00	0.03	0.92	0.00	0.05	0.04	0.00	0.05	0.00	0.12
MgO	11.05	8.92	9.54	0.00	0.00	0.00	0.00	0.00	0.07	0.04	0.02
FeO	18.28	19.67	19.37	10.51	0.24	0.18	0.07	0.11	19.31	19.62	18.24
MnO	1.43	0.36	0.32	11.87	0.05	0.07	0.00	0.03	1.73	1.92	1.68
CaO	11.13	11.84	11.92	0.20	9.80	9.48	5.64	5.97	29.71	29.87	29.59
Na_2O	1.21	1.09	0.83	23.09	5.90	6.21	8.11	8.22	0.00	0.00	0.00
K_2O	0.73	0.53	0.34	0.35	0.10	0.08	0.27	0.16	0.02	0.00	0.00
H_2O	1.98	1.98	2.00	0.05					2.58	2.59	2.57
Total	99.50	99.82	100.08	99.98	99.76	100.95	100.10	99.89	100.36	100.88	99.50
Si	6.676	6.577	6.948	1.976	2.511	2.521	2.697	2.693	19.186	19.162	19.038
Ti	0.027	0.055	0.046	0.005	0.000	0.002	0.000	0.000	0.507	0.388	0.272
Al	1.422	1.879	1.447	0.038	1.488	1.478	1.317	1.309	5.421	5.547	6.245
Cr	0.007	0.012	0.012	0.004	0.000	0.001	0.000	0.000	0.037	0.000	0.062
Fe^3	1.159	0.650	0.469	0.026							
Ni	0.000	0.000	0.004	0.000	0.000	0.002	0.001	0.000	0.021	0.000	0.051
Mg	2.432	1.981	2.106	0.597	0.000	0.000	0.000	0.000	0.055	0.031	0.016
Fe^2	1.098	1.801	1.929	0.378	0.009	0.007	0.003	0.004	8.440	8.542	7.994
Mn	0.179	0.045	0.040	0.006	0.002	0.003	0.000	0.001	0.766	0.847	0.746
Ca	1.761	1.890	1.891	0.942	0.474	0.452	0.268	0.285	16.638	16.661	16.615
Na	0.346	0.315	0.238	0.026	0.516	0.536	0.698	0.710	0.000	0.000	0.000
K	0.138	0.101	0.064	0.002	0.006	0.005	0.015	0.009	0.013	0.000	0.000
OH									9.000	9.000	9.000
Total	15.245	15.306	15.194	4.000	5.006	5.007	4.999	5.011	60.084	60.178	60.039
X_{Fe}	0.311	0.476	0.478	0.388					0.994	0.996	0.998
F^3min	3.83	2.80	1.21								
F^3max	13.39	11.41	7.77								
FS13	10.43	5.80	4.21	X_{An}	0.48	0.46	0.27	0.28			
FS15	13.39	11.41	7.77	X_{Ab}	0.52	0.54	0.71	0.71			
fHB	1.0046	0.9998	0.9998	X_{or}	0.01	0.00	0.02	0.01			

BLN282 (amphibolite): amphibole, clinopyroxene and plagioclase. BLN277a (metarhyolite): amphibole, plagioclase and vesuvianite.
FS13 and FS15: Structural formula with 13 and 15 cations, respectively. fHB: correction factor to comply with Holland & Blundy (1984) geothermometer.

Geochronology

Virtually no zircons have been found in the amphibolites or the metarhyolites. This is due to their mylonitic fine-grained texture. Indeed, zircons are very difficult to separate when they are small (10–20 μm), their volume being too limited to allow their separation by difference of density. Ar–Ar, Rb–Sr and Sm–Nd geochronometers were used. For the three methods, all ages are stated with errors at the 2σ level (95% confidence).

Analytical techniques

Ar-Ar. The dated sample (BLN73a) is an amphibole separate from a mylonitized amphibolite sampled along the eastern margin of the Tchilit terrane (Fig. 3). A green hornblende concentrate was obtained from a 65–105 μm magnetic fraction and further purified by handpicking up to a 99% (based on optical evaluation) degree of purity. Minute feldspar (plagioclase) grains remain adhered to the hornblende grains.

The hornblende sample together with aliquots of HD-B1 and LP-6 biotite standards, CaF_2 and K_2SO_4 salt monitors were irradiated under Cd-shielding in the BR2-reactor of the Nuclear Research Centre at Mol, Belgium. Step ages are calculated with a J-factor=0.1004 ± 0.0054, obtained from cross-calibration measurements on two age standards: the biotite HD-B1 with a used reference age of 24.21 ± 0.32 Ma (Hess & Lippolt 1994) and LP-6 biotite for which Baksi *et al.* (1996) reported a reference age of 128.1 ± 0.2 Ma. The errors in the apparent step-ages (2σ) as stated in Table 2 and in Fig. 5 account for the analytical errors including the variability of the neutron flux. The uncertainty in the J-factor resulting from standard interaliquot variability is estimated at 1% but excludes errors on the K and Ca correction factors.

All gas extractions were accomplished with an induction furnace. The sample was progressively step-wise heated in a tantalum crucible. Step-temperatures are determined with a 5%W/Re–26% W/Re thermocouple. Released gases were purified by exposure to a Ti-getter within a T° gradient and to heated and cold Zr–Al getters, before isotopic measurement in a MAP 216 mass spectrometer operated in static mode. The MAP 216 is equipped with a Bauer-Signer source, a Johnston electron multiplier and a retractable Faraday cup. ^{40}Ar, ^{39}Ar, ^{38}Ar, ^{37}Ar and ^{36}Ar isotopic abundances were determined through linear extrapolation at time zero of peak intensities during fifteen sequential scans. These data were corrected for

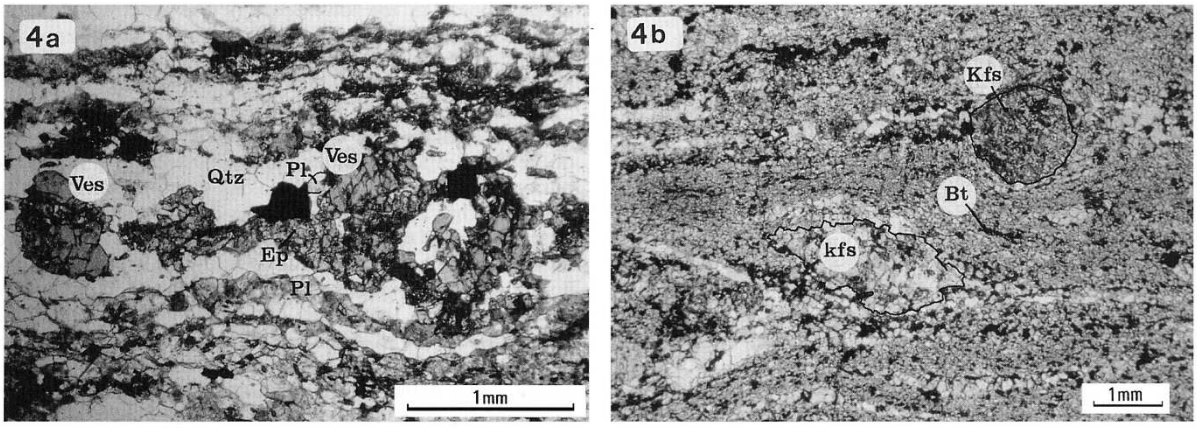

Fig. 4. Microphotographs of the textural relationships in the studied rocks. (**a**) Polycrystalline aggregates of vesuvianite (Ves)–plagioclase (Pl)–quartz (Qtz)–magnetite with secondary epidote (Ep) (sample BLN 277b). (**b**) Polycrystalline aggregates and porphyroclasts of K-felsdspar (Kfsp) in mylonitic metarhyolites coexisting with biotite (Bi), quartz and magnetite (sample BLN 277c).

Table 2. Ar–Ar stepwise heating results on a hornblende separate (sample BLN73) from a mylonitic amphibolite along the eastern margin of the Tchilit terrane

Temp. (°C)	$^{40}Ar/^{39}Ar$	$^{37}Ar/^{39}Ar$	$^{36}Ar/^{39}Ar$ ($\times 10^{-3}$)	$^{38}Ar/^{39}Ar$ ($\times 10^{-3}$)	$^{37}Ar/^{38}Ar$	^{39}Ar Cum (%)	$^{40}Ar^*$ (%)	$^{40}Ar^*/^{39}Ar$	Ca/K	Apparent age ± 1 s.d. (Ma)
680	285.04	3.24	897.64	191.34	16.95	6.89	6.57	18.74	6.53	1910 ± 86
900	5.84	12.33	9.30	16.36	753.55	57.28	66.71	3.90	25.30	606 ± 10
960	8.92	11.03	9.21	14.30	771.24	61.46	77.57	6.92	22.70	967 ± 88
1000	9.78	12.69	16.29	17.15	739.81	68.72	59.34	5.81	26.10	846 ± 62
1050	11.93	12.90	19.86	17.38	742.06	74.39	57.80	6.90	26.50	969 ± 76
1110	13.88	12.67	25.34	16.72	757.73	78.92	51.80	7.19	26.10	1000 ± 98
1160	16.89	12.26	32.74	21.79	562.77	83.06	47.60	8.04	25.00	1080 ± 104
1200	30.64	11.72	67.00	23.91	490.14	85.38	37.86	11.60	24.00	1410 ± 164
1230	27.51	11.96	62.32	23.09	518.13	88.65	35.78	9.84	24.70	1260 ± 126
1250	32.526	11.70	78.19	26.40	443.00	91.71	31.29	10.18	24.00	1290 ± 135
1320	31.154	12.02	76.25	28.46	422.30	95.77	30.15	9.39	24.70	1220 ± 105
1400	72.544	11.43	196.50	49.80	229.46	98.67	20.59	14.94	23.40	1680 ± 119

mass discriminations, interfering Ca, K, and Cl derived argon isotopes, and the decay of ^{37}Ar and ^{39}Ar since the time of irradiation. Decay constants used throughout the calculations are those recommended by Steiger & Jäger (1977).

Rb–Sr and Sm–Nd. After acid dissolution of the sample and Sr and/or Nd separation on ion-exchange resin, Sr isotopic compositions have been measured on Re double filament (Finnigan MAT 260) or Ta simple filament (VG Sector 54) and Nd isotopic compositions on triple Ta–Re–Ta filament (VG Sector 54). Repeated measurements of Sr and Nd standards have shown that between-run error is better than 0.00004 on the MAT 260 and better than 0.00002 on the Sector 54. These errors have been chosen in the calculations for the general case where the within-run errors are lower. The NBS987 standard has given a value for $^{87}Sr/^{86}Sr$ of 0.710240 ± 0.000005 (2σ on the mean, 35 measurements, normalized to $^{86}Sr/^{88}Sr=0.1194$) and the MERCK Nd standard a value for $^{143}Nd/^{144}Nd$ of 0.512740 ± 0.000005 (2σ on the mean, 26 measurements, normalized to $^{146}Nd/^{144}Nd=0.7219$) during the course of this study. Rb and Sr concentrations have been measured by X-ray fluorescence or by isotope dilution when concentrations were <30 ppm. The error on the Rb/Sr ratio is <2%. Sm and Nd concentrations were measured by ICP–MS. The error on the Sm/Nd ratio is <2%. The Rb–Sr and Sm–Nd ages have been calculated following Williamson (1968). Used decay constants (Steiger & Jäger 1977) are 1.42×10^{-11} a^{-1} (^{87}Rb) and 6.54×10^{-12} a^{-1} (^{147}Sm). Sr and Nd isotope ratios can be found in Table 3.

Results

Ar–Ar. The Ar–Ar age and Ca/K spectra are shown in Fig. 5, the corresponding analytical results are listed in Table 2. Throughout the whole stepwise-heating experiment the Ca/K ratio deduced from the isotopic composition of the released argon remains fairly stable, although a slight stair-case decrease in the spectrum is observed starting from extraction temperatures above 1050°C. The first step yields a much lower Ca/K ratio. This pattern can be explained by the presence of small impurities (plagioclase) in the analysed hornblende sample. The small impurities have, relative to the hornblende composition, higher K and/or lower Ca contents. Because of their finer grain size and different composition they would preferentially outgas at low temperatures. The value (about 25) obtained for the Ca/K ratios, is comparable to microprobe results obtained on other but representative amphibole separates used for thermometry analysis (Table 1).

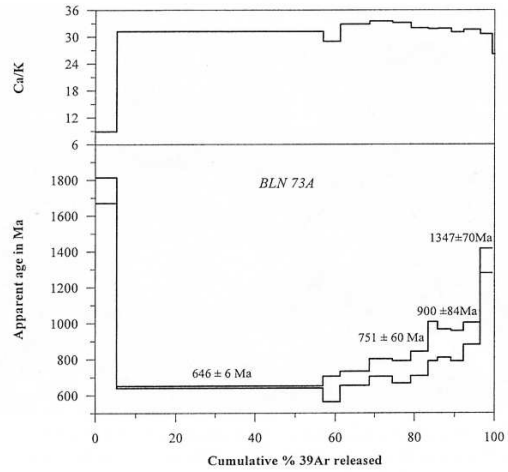

Fig. 5. Ar–Ar age and Ca/K spectra of hornblende separate (sample BLN73) from a mylonitic amphibolite from the Tchilit terrane.

The age spectrum itself displays a marked discordance. Argon released during the lowest extraction temperature yields (with a rather large error because of the high proportion of common argon in sites with low degree of retentivity) an apparent age of 1772 ± 72 Ma. However the next step accounts for as much as 50% of the total released ^{39}Ar and gives an apparent age of 646 ± 6 Ma. Subsequent steps define roughly a staircase spectrum with an increase in apparent ages, up to a maximum of 1347 ± 70 Ma. It is likely that irregularities would appear in the lower part of the spectrum if argon had been released in more steps. Nonetheless, its apparent age is much lower than that corresponding to higher temperature parts.

No biotite impurities, which could be at the origin of such a spectrum (Wartho 1995), have been observed. The constancy of the Ca/K ratio (except for the lowest stepage) confirms the purity of the amphibole separate. As only one generation of amphibole has been observed in the mineral concentrate, the interpretation of this spectrum in terms of mixing between two different amphiboles can be ruled out. In the present case, the notion of excess argon does not impose itself. We therefore have to consider that argon escaped more easily from the hornblende lattice in distinctive parts or along fast pathways (Villa *et al.* 1996). In that case, the lowest apparent step age is considered as dating a thermal event that produced the argon loss from the less retentive sites of the samples (Harrison 1981; Kelley & Turner 1991). The 646 ± 6 Ma age (Fig. 5) is therefore interpreted as a Pan-African overprinting onto a much older (>1400 Ma) hornblende. This indicates that not only the protolith, but also the amphibolite facies metamorphism, which produced the hornblende, is older than 1400 Ma. The low temperature age corresponds to the major regional but discrete greenschist high-temperature metamorphic phase accompanied by high-K calc-alkaline granitoids in the Assodé terrane, that was bracketed between 645 and 580 Ma (Liégeois *et al.* 1994). Whether the inferred event actually reflects a thermal disturbance at a regional scale due to the emplacement of the syenogranites observed in the Tchilit terrane (619 ± 39 Ma, see below), or rather to the deformational process related to the mylonitization remains an open question as both phenomena are subcontemporaneous.

Table 3. *Sr and Nd isotopic ratios and calculations for Tchilit terrane*

Sample no.	Rb (ppm)	Sr (ppm)	$^{87}Rb/^{86}Sr$	$^{87}Sr/^{86}Sr$	2σ	Sm (ppm)	Nd (ppm)	$^{147}Sm/^{144}Nd$	$^{143}Nd/^{144}Nd$	2σ	Sr_i	ε_{Nd}	T_{DM}
Amphibolites											2100 Ma		
BLN280	3.6	296	0.0352	0.714842	0.000009	4.02	17.18	0.1414	0.511192	0.000014	0.71378	−13.4	4060
BLN282	58.5	355	0.4772	0.716207	0.000009						0.70181		
BLN285	7.6	290	0.0760	0.717503	0.000010						0.71521		
BLN287	4.2	531	0.0229	0.713247	0.000009	3.87	16.8	0.1392	0.511320	0.000009	0.71256	−10.3	3628
BLN288	2.8	273	0.0301	0.716522	0.000010						0.71563		
BLN73	21.3	299	0.2058	0.718472	0.000030	4.8	20.3	0.1429	0.511566	0.000019	0.71224	−6.5	3249
BLN78	3.2	451	0.0208	0.709600	0.000011						0.70898		
BLN81	11	554	0.0574	0.713158	0.000050	5.4	24.02	0.1360	0.511492	0.000014	0.71143	−6.0	3088
Rhyolites											1800 Ma		
BLN74	220	126	5.1217	0.849290	0.000030						0.71665		
BLN75	128	111	3.3652	0.796202	0.000030	16	85	0.1138	0.511184	0.000011	0.70905	−9.3	2863
BLN79	129	342	1.0956	0.747951	0.000040	14	83	0.1019	0.511011	0.000006	0.71958	−9.9	2794
BLN80	179	303	1.7193	0.768233	0.000040						0.72371		
BLN276	150	77.6	5.6732	0.854995	0.000010						0.70807		
BLN277a	148	114	3.7913	0.803311	0.000008	14	72	0.1175	0.511202	0.000011	0.70513	−9.8	2951
Granites											619 Ma		
BLN272	307	193	4.6215	0.750592	0.000011	7.5	47	0.0964	0.511067	0.000014	0.70978	−22.8	2582
BLN274	281	244	3.3425	0.739929	0.000011	9.6	61	0.0951	0.511449	0.000008	0.71041	−15.2	2050
BLN281	321	97.3	9.6271	0.795568	0.000011	8.1	41	0.1194	0.511453	0.000018	0.71055	−17.0	2587
Quartzite													
BLN82	60.2	38.2	4.5934	0.783571	0.000040						0.74301		
Conglomerate													
BLN83	129	241	1.5531	0.736819	0.000030						0.72311		

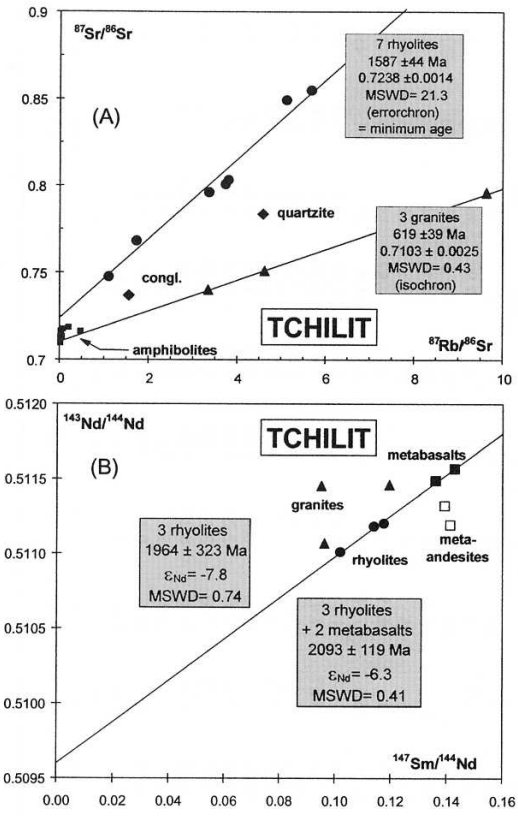

Fig. 6. (**a**) $^{87}Rb/^{86}Sr$ versus $^{87}Sr/^{86}Sr$ diagram showing the errorchron defined par the metarhyolites (minimum age for amphibolite facies metamorphism and extrusion) and the isochron defined by the granite (intrusion age). The monophased metasediments are probably Neoproterozoic in age. (**b**) $^{147}Sm/^{144}Nd$ versus $^{143}Nd/^{144}Nd$ diagram showing the isochron defined by the metarhyolites. The metabasalts lie on this isochron suggesting emplacement during the same Palaeoproterozoic orogeny but not necessarily their strict contemporaneity.

Rb–Sr. Unfortunately, only three syenogranite samples are available. They are well aligned, defining an isochron with an age of 619 ± 39 Ma ($Sr_i = 07103 \pm 0.0025$, MSWD=0.43, Fig. 6a) which is in the same age range as the greenschist metamorphism and the high-K calc-alkaline granitoids of the Assodé terrane (645–580 Ma; Liégeois *et al.* 1994). This late Pan-African age is in agreement with the unmetamorphozed and undeformed nature of this syenogranite and corresponds probably to the end of the thrusting event. A crustal input in its genesis is indicated by its relatively high initial ratio (0.710).

The metarhyolites define a trend (1587 ± 44 Ma, Sr initial ratio (Sr_i)=0.7238 ± 0.0014, MSWD=21.3 for 7 whole rocks; Fig. 6a) which cannot be considered as an isochron because of the high MSWD value. This age is geologically meaningless. The 1587 age can however, be interpreted as an intermediate value between the Pan-African perturbation (646 ± 6 Ma, Ar–Ar and 619 ± 39 Ma, Rb–Sr on the syenogranite) and the amphibolite-facies metamorphism. The existence of this Rb–Sr errorchron giving an old age confirms that the Pan-African overprinting was rather weak, hardly compatible with an amphibolite-facies metamorphism. Taking the mean Rb/Sr ratio of the metarhyolites, the maximum age obtained for this event and for the eruption of the rhyolites themselves, is 2162 Ma (mean $^{87}Rb/^{86}Sr = 3.4$; $Sr_i = 0.701$). As the mean $^{87}Rb/^{86}Sr$ is rather high, this maximum age is not greatly affected by the chosen mean nor by the chosen initial ratio. Then, even disturbed by the Pan-African metamorphism, the Rb–Sr chronometer indicates that the rhyolites were emitted and affected by the amphibolite facies metamorphism between 1587 Ma and 2162 Ma. The very notion of exotic terrane urges on caution and on leaving open, within the 1587–2162 Ma bracket, the precise age of this amphibolite metamorphism. This point will be discussed below with geochemical and initial isotopic data. Whatever, this gives plenty of time for the deposition of the detrital sediments, affected only by the Pan-African greenschist metamorphism. Their position in the Rb–Sr isochron diagram (Fig. 6a) suggests that these sediments are roughly Neoproterozoic in age.

The amphibolites are Rb-poor and show a scattered distribution (Fig. 6a). No geochronological information can be deduced.

Sm–Nd. The three analysed metarhyolites define an imprecise isochron: 1964 ± 323 Ma ($\varepsilon_{Nd} = -7.8 \pm 1$, MSWD= 0.74, Fig. 6B), an age range (1641–2287 Ma) which corresponds to the Rb–Sr 1587–2162 Ma calculated time span. To the contrary, the amphibolites do not determine an isochron. The two metabasalts lie on the metarhyolite isochron giving: 2093 ± 119 Ma ($\varepsilon_{Nd} = -6.3 \pm 0.5$, MSWD=0.74, 5 whole rocks, Fig. 6b). The validity of this 'age' cannot be assessed and it suggests only that the metabasalts and the metarhyolites could belong the same Palaeoproterozoic orogenic cycle. The two meta-andesites plot below the isochron suggesting crustal involvement during differentiation of the basalts. The two analysed syenogranites give low ε_{Nd} values between -15 and -23 at 619 Ma indicating an essentially crustal origin.

Geochemistry and isotope geochemistry

Analytical techniques

Major elements. Si, Al, Ti, Fe, Ca and P have been analyzed by X-ray fluorescence following the method described by Norrish & Hutton (1969); Mn, Mg, K and Na have been measured by atomic absorption after open acid digestion ($HF + HClO_4 + HNO_3$); FeO has been titrated by permanganametry.

Trace elements. Three different techniques have been used for the analysis of 29 trace elements: X-ray fluorescence on raw material for Rb and Sr; ICP-AES for Cu, Zn, Cr and Co (for details, see Navez 1983); ICP-MS (VG PQ2+) for the other elements: the result of the alkaline fusion (0.3 g of sample +0.9 g of lithium metaborate at 1000°C during one hour) has been dissolved in 5% HNO_3. The calibrations were set using both synthetic solution (mixture of the considered elements at 2, 5 and 10 ppb) and international rock standards (BHVO-1, W1, GA, ACE). For all these elements, the precision varies from 5 to 10% (for details, see Navez 1995).

Major and trace elements can be found in Table 4.

Results

Amphibolites. The amphibolites fall in the low-K calc-alkaline field (Fig. 7a), having too low FeO* and FeO*/MgO values to

Table 4. *Major and trace elements for Tchilit terrane*

	Rhyolites					Amphibolites											Granites		
	BLN75	BLN79	BLN277a	BLN276	BLN74	BLN72	BLN73	BLN78	BLN81	BLN285	BLN287	BLN280	BLN282	BLN286	BLN288	BLN292	BLN272	BLN274	BLN281
SiO_2	66.53	71.56	71.86	73.55	66.43	55.89	51.05	53.39	50.7	56.91	57.36	55.44	53.52	57.57	57.13	47.66	72.98	70.94	75.6
TiO_2	0.97	0.59	0.83	0.36	0.92	0.48	1.32	0.61	1.64	0.65	0.63	0.66	0.68	0.51	0.63	1.94	0.42	0.48	0.13
Al_2O_3	13.39	12.91	11.33	12	12.98	12.65	13.74	13.65	13.66	15.49	15.44	15.6	13.34	15.45	15.75	13.78	14.82	14.79	13.77
Fe_2O_3	3.61	2.2	3.02	2.06	3.13	4.89	4.39	1.38	10.02	3.39	2.05	2.2	2.11	2.54	1.9	4.6	1.53	1.95	0.78
FeO	2.19	1.88	2.07	0.9	2.43	3.51	8.94	5.93	5.78	5.12	5.36	6.75	5.54	4.63	5.86	11.51	0.17	0.76	0.34
MnO	0.13	0.08	0.09	0.04	0.38	0.2	0.63	0.15	0.24	0.14	0.12	0.14	0.12	0.13	0.13	0.22	0.03	0.07	0.06
MgO	0.68	0.39	0.59	0.14	0.76	5.99	5.1	4.39	5.31	5.37	4.37	5.64	4.47	4.21	5.37	6.14	0.4	0.66	0.14
CaO	2.61	2.85	1.53	0.9	2.25	6.86	9	17.12	7.83	7.84	12.75	7.99	13.28	10.05	7.5	10.02	0.92	1.32	0.86
Na_2O	3.59	2.38	2.01	2.53	2.39	6.78	3.28	0.48	2.45	3.86	1.26	4.34	2.24	3.32	4.87	1.81	3.3	3.34	3.22
K_2O	4.63	3.06	4.94	5.15	5.98	0.44	0.42	0.17	0.25	0.3	0.21	0.26	1.15	0.73	0.18	0.38	5.18	4.94	5.23
P_2O_5	0.29	0.17	0.29	0.08	0.3	0.28	0.16	0.11	0.19	0.12	0.1	0.1	0.11	0.09	0.09	0.16	0.14	0.19	0.06
P.F.	1.48	2.91	1.27	0.98	1.52	0.94	1.74	2.21	1.26	1.02	1.31	1.19	1.61	1.22	1.03	1.79	0.83	0.74	0.46
Total	100.1	100.98	99.84	98.7	99.48	98.91	99.77	99.61	99.33	100.21	100.96	100.3	100.16	100.44	100.44	100.01	100.73	100.18	100.64
Fe tot	6.04	4.29	3.52	3.06	5.83	8.79	14.31	7.97	16.44	9.08	8.01	9.68	8.26	7.68	8.4	2.84	1.72	2.8	1.15
Rb	128	129	148	150	199	14.6	22	2.8	10	7	4	4.8	52	12.7	2	5.9	307	281	321
Sr	111	342	114	78	126	1082	299	451	554	290	531	296	355.4	484.6	273	198.4	193	244	97
Y	74	63	72	69	85	14.6	27	17.8	33	23	22	20	18.2	15.2	18	37	40	42	41
Zr	441	372	566	558	426	77	144	97	161	93	89	91	92	62	86	135	240	362	123
Cu	15	17	3	3	11	95	143	28	195	14	38		29	18	30	169	20	10	2
Zn	166	131	95	94	179	194	161	138	181	98	73		70	74	95	15	55	78	42
V	47	29	25	7	47	188	307	205	379	122	114	122	114	111	96	280	21	29	6.9
Cr	14	16	2	1	13	241	75	79	95	74	71		79	59	73	105	0.001	1	2
Co	8.4	6.2	6.1	2.3	11	31	55	41	58	34	39	40	41	30	32	47	8	6	1.5
Nb	35	34	34	35	34	3.34	7.2	4.4		4.6	4.6	4.7	4.9	2.9	4.5	7.9	36	38	35
Ba	1012	1568	1173	1129	1438	1137	99	66	514	150	166	40	115	271	70	78	856	900	327
La	109	128	95	145	108	14.2	19	16.9	26	14.9	16.2	15.9	16	13.8	16	14.5	84	107	51
Ce	212	239	183	268	215	27	43	33	51	33.9	35	36	35	29	33	33	149	183	98
Pr	23	24	20	27	25	3.23	5.1	4.01	6	3.99	4.1	4.19	4.08	3.37	4.12	4.67	15	19	11.6
Nd	85	83	72	91	93	13.2	20	16.1	24	16.5	16.8	17.18	16.7	13.8	16.8	21.4	47	61	41
Eu	3.4	2.4	2.8	1.8	3.19	0.75	1.5	1.25	1.7	1.18	1.17	1.2	1.32	0.93	1.12	1.84	1.3	1.7	0.77
Sm	16	14	14	15	15.8	2.26	4.8	3.24	5.4	3.94	3.87	4.02	3.81	3.08	3.9	6.26	7.5	9.6	8.1
Gd	15	13	14	14	15.1	2.7	5.2	3.17	6.1	3.92	3.83	3.87	3.64	3.11	3.83	7.28	6.9	8.6	6.9
Dy	14	12	13	12	15.2	2.51	5.2	3.19	5.9	3.95	3.71	3.97	3.71	3.06	3.91	7.68	5.5	6.8	7
Ho	3.1	2.6	2.8	2.7	3.3	0.53	1.2	0.66	1.3	0.86	0.8	0.85	0.8	0.66	0.84	1.65	1.2	1.5	1.63
Er	9.5	8	8.5	8.2	9	1.44	3.5	1.84	3.67	2.34	2.19	2.37	2.23	1.82	2.32	4.52	4.1	4.5	4.31
Yb	8.6	7.6	7.8	7.4	8.6	1.35	3	1.79	3.6	2.42	2.22	2.43	2.23	1.88	2.38	4.45	4.1	4.4	4.68
Lu	1.3	1.1	1.2	1.1	1.3	0.21	0.45	0.27	0.52	0.36	0.34	0.37	0.34	0.29	0.37	0.66	0.64	0.68	0.71
Hf	17	15	15	15	16.6	2.33	4	2.43	4.2	3.1	2.9	2.9	3	2.1	3.1	4.6	8.2	9.4	4.29
Ta	2.3	2.5	2.1	2.4	2.23	0.19	0.83	0.34	0.66	0.39	0.38	0.4	0.43	0.31	0.4	0.62	3.1	3.2	3.27
W	2.1	1.1	1.6	0.74	0.9	0.79	1.5	1.47	1.2	0.2	0.6	0.4	0.7	0.3	0.5	0.6	5	0.93	0.8
Pb	61	42	62	50	36	15.8	35	8.2	21	8	9.8	7.7	9	9.8	11.2	9.9	98	69	57
Th	25	33	22	37	28	1.22	4.2	2.89	4.6	3.44	3.3	3.42	3.63	2.75	3.6	2.9	43	41	61
U	5.4	6.1	4.5	7.5	4.8	0.43	0.85	0.8	0.91	0.85	0.88	1.04	1.02	0.83	1.12	0.5	17	10	14.4

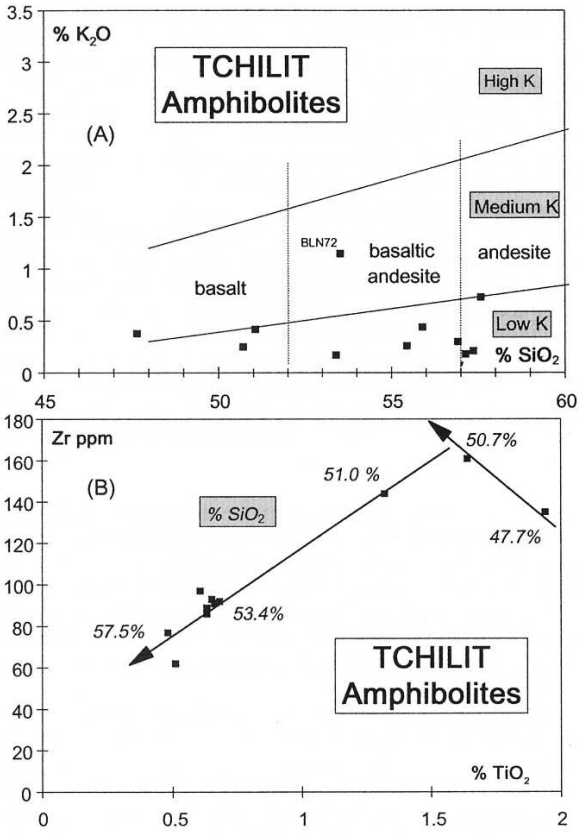

Fig. 7. Major element geochemistry of Tchilit amphibolites (**a**) SiO_2 versus K_2O diagram: the amphibolites define a low-K calc-alkaline trend from basalts to andesites (BLN72, sampled at the Tafadek hot springs is more altered). Congl., conglomerate. (**b**) TiO_2 versus Zr diagram showing that TiO_2 is compatible until 47.7% SiO_2 while Zr saturation occurred only at *c.* 51% SiO_2.

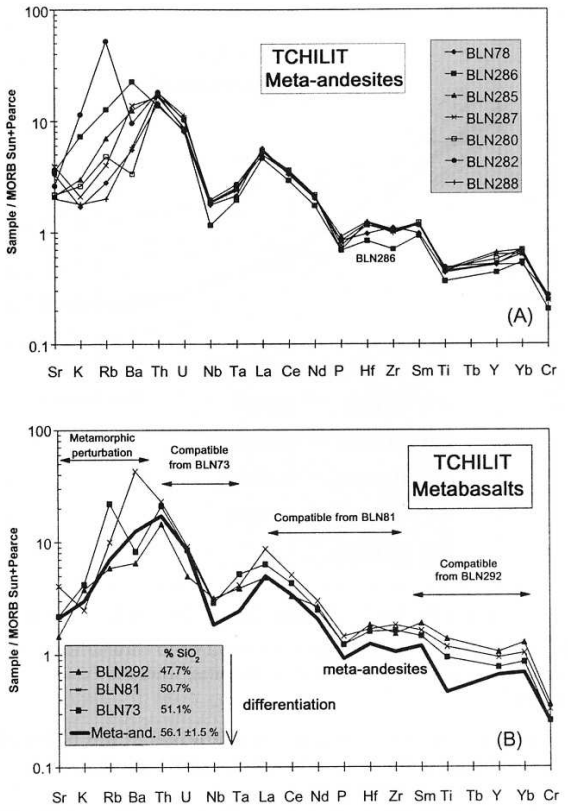

Fig. 8. Spidergrams normalized to N-MORB (Pearce 1982 and Sun 1980). (**a**) Andesitic amphibolites: elements from Th to Cr show an immobile behaviour during metamorphism by opposition to Sr, K, Rb and Ba. (**b**) All amphibolites: the four left elements have been altered by metamorphism; the other elements display an increasing degree of compatibility to the left during differentiation in agreement with their theoretical magmatic behaviour.

belong to the tholeiitic series (Miyashiro 1974). Three basalts, four basaltic andesites and four andesites may be identified. The latter eight will be grouped under the name meta-andesites hereafter. The BLN72 sample has an abnormally high K_2O and Rb values suggesting the effects of metamorphic fluids. All the rocks have very low Cr contents precluding any significant amount of cumulative minerals. They can be considered as representing liquids. The binary diagram TiO_2 versus Zr (Fig. 7b) illustrates the difference of compatibility degree of these elements: TiO_2 was already compatible at 47% SiO_2 (TiO_2=1.9%) while the saturation of Zr occurred at around 51% SiO_2 (TiO_2=1.7%) at a value of 160 ppm Zr. This is a magmatic feature. The magmatic or metamorphic origin of the element concentrations in Tchilit rocks can be checked globally for other elements through spidergrams.

In a MORB normalized spidergram, seven meta-andesites have a very similar pattern for the 15 elements ranging from Th to Cr (Fig. 8a), only BLN286 is slightly below the others due to a more differentiated character (BLN72 sampled at the Tafadek hot springs has been more altered (Fig. 7a) and has been omitted here). In contrast, the four elements on the left (Sr, K, Rb, Ba) are very scattered reflecting mobility in aqueous fluids due to their high ionic potential (Pearce 1982). This scattering can be attributed to metamorphism. These elements cannot then be used to characterize the protolith of the amphibolites. In contrast, the elements to the right of Th were immobile and can represent the initial magmas. In Fig. 8b, the three metabasalts have been added to the mean of the meta-andesites (excluding BLN286) represented by a thick single line. On this diagram, the magmatic behaviour of the elements (except for Sr, K, Rb and Ba) can be followed during the differentiation. That is, from the least to the most differentiated: BLN292 (47.7% SiO_2), BLN81 (50.7% SiO_2), BLN 73 (51.1% SiO_2) and the meta-andesites (56.1 ± 1.5% SiO_2). From this succession, it appears that the theoretical compatibility (decreasing from Cr to Th) is well respected: elements from Cr to Sm are compatible already at 47% SiO_2, from Zr to La at 50% SiO_2 and from Ta to Th at 51% SiO_2 (Fig. 8b). This feature is also shown by the REE (Fig. 9a and b): HREE are continuously decreasing (Yb_N or Lu_N from 20 to 6) while LREE increase from 47% to 51% SiO_2 (La_N from 50 to 80) and afterward decrease (down to 40 for La_N). The more primitive metabasalt has the most pronounced negative Eu anomaly. The other rocks have only slight negative Eu anomalies except two samples with positive anomalies (slight in BLN282, higher in BLN78). This indicates that if the plagioclase was an early cumulative phase (in the parent magma at the origin of the

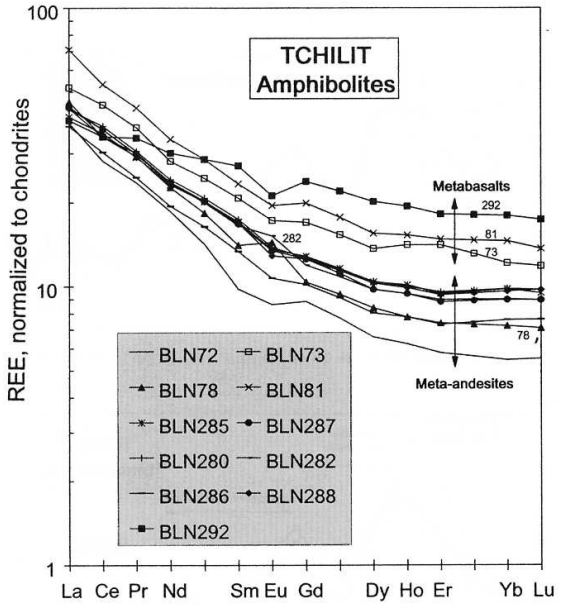

Fig. 9. Rare earth element patterns normalized to chrondrites of the amphibolites (metabasalts and meta-andesites) from the Tchilit terrane.

series), its fractionation was minor afterwards or was balanced by a cumulative mineral with an Eu negative anomaly such as an amphibole or a pyroxene.

The 15 elements from Cr to Th can then be used to determine the palaeogeodynamic setting of the protoliths. The three metabasalts have compositions probably close to the parental magma while the meta-andesites show the effects of the differentiation. The overall spectrum (Fig. 8b) shows a Nb–Ta anomaly typical for active margin calc-alkaline rocks, the values around 1 for the elements between P and Yb and the enrichment from P to La suggesting a continental margin. In the Yb versus Ta diagram (Fig. 10a), all the Tchilit amphibolites fall in the arc domain, with the differentiation trend moving away from the within plate and MORB fields. We note that the metarhyolites are at the opposite end of this differentiation trend: the two volcanic groups in Tchilit are not genetically linked. In the Ti/100–Zr–Y*3 (Fig. 10b), all amphibolite samples but one are in the exclusive volcanic continental arc field. The exception, the more primitive BLN292 metabasalt, is in the common field of oceanic volcanic arc and MORB. In the other triangular diagram (La/10–Y/15–Nb/8, Fig. 10c), the Tchilit samples fall in the calc-alkalic basalt field, clearly outside of the MORB and tholeiitic fields. Again, the primitive metabasalt BLN292 indicates a more pronounced MORB or back-arc-basin signature. This is probably not a within-plate enrichment which would affect Nb more than Y (as shown by the intracontinental rift alkali basalt field). The diagram Ta/Yb versus Th/Yb (Fig. 10d) constitutes a good summary: the Tchilit amphibolites are within the calc-alkaline active continental margin domain (as the Andes) with the most primitive metabasalts closer to the MORB field. The Tchilit amphibolites represent then a tiny portion of a Palaeoproterozoic continental active margin.

Calculation of Sr initial ratios (Table 3) is weakened by the likely modification of the Rb/Sr ratios during Pan-African metamorphism. However, due to low Rb/Sr ratios, except for sample BLN282 which has been strongly enriched in Rb (Fig. 8a), this does not greatly influence the calculated values which pass from 0.710–0.718 (present measured values) to 0.709–0.715 at 2100 Ma (Fig. 11). These rather high values, coupled with the ε_{Nd} (-6 for metabasalts, -10 and -13 for meta-andesites, Fig. 11, Table 3) indicate a significant crustal input probably growing with the differentiation. The crustal contamination is in agreement with a continental margin environment and excludes an oceanic setting comparable to the contemporaneous Birimian oceanic mega-island arc in the West African craton (Ama Salah *et al.* 1996). The T_{DM} model ages between 3090 Ma and 4056 Ma (Table 3) indicate an old Archaean crust as the contaminant. Such a crust exists to the north in Hoggar (Egéré–Aleksod terrane, Fig. 1) where granulitic banded gneisses from a metasedimentary sequence have been dated at 3480 ± 90 Ma (Latouche & Vidal 1974). Early Archaean rocks (>3.1 Ga) have also been dated to the south in Nigeria (Bruguier *et al.* 1994).

Metarhyolites. The metarhyolites are enriched in high field strength elements (Fig. 12a) and in heavy rare earth elements (Fig. 12b). Their ORG-normalized spidergrams are similar to that of a typical alkaline ring-complex (Mull, Pearce *et al.* 1984). Steep LREE with La_N between 300 and 400, strong Eu negative anomaly, horizontal and high HREE (Yb_N between 30 and 40) as well as Yb and Ta abundances (Fig. 10a) point also to an alkaline character.

The metarhyolites do not show significant mobility of Rb, Sr, K and Ba as in the amphibolites, except maybe BLN79, which seems to be abnormally depleted in Sr and Rb and enriched in Ba. However, as shown on the Rb–Sr isochron diagram (Fig. 6a), the Rb/Sr and $^{87}Rb/^{86}Sr$ ratios were probably modified during metamorphism, introducing some uncertainties on the calculated Sr initial ratios. Calculated strontium initial ratios are between 0.715 and 0.732 at 1600 Ma, 0.702–0.713 at 1850 Ma (0.719 for the more tectonized BLN79). At 2100 Ma, the global mean is *c.* 0.702 with several samples below 0.7 showing that this is a maximum age for the metarhyolites (Fig. 11)

The ε_{Nd} values (Table 3; Fig. 11) indicate a crustal input in the genesis of the metarhyolites ($\varepsilon_{Nd} = -6.5$ at 2100 Ma and -10 at 1800 Ma), intermediate between the metabasalts (-6 at 2100 Ma) and the meta-andesites (-10 and -13). A mixed juvenile/old signature is most likely for these rhyolites. The T_{DM} model ages between 2793 Ma and 2949 Ma (Table 3) indicate, as for the amphibolites, that the old crustal component is Archaean in age and probably corresponds to the same deep crust.

Whether the rhyolites have been generated in the same geotectonic setting as the amphibolites cannot be solved without precise dating of both lithologies. Their sources are different but they have been subjected to the same Palaeoproterozoic amphibolite-facies metamorphism. The low-K calc-alkaline signature of the amphibolites indicates a continental active margin. The alkaline geochemistry of the rhyolites is less sensitive to the geotectonic setting. If regional correlations are tempted, the amphibolites could be the equivalent of the Birimian oceanic island arc (Ama Salah *et al.* 1996) but located on a continental margin, and would belong in that case to the Eburnian orogeny (2.1 ± 0.1 Ga; Liégeois *et al.* 1991). The rhyolites could also be related to an Eburnian post-collisional event. On the other hand, they can also be correlated with the alkaline gneisses dated at around 1.8 Ga in the West Tuareg

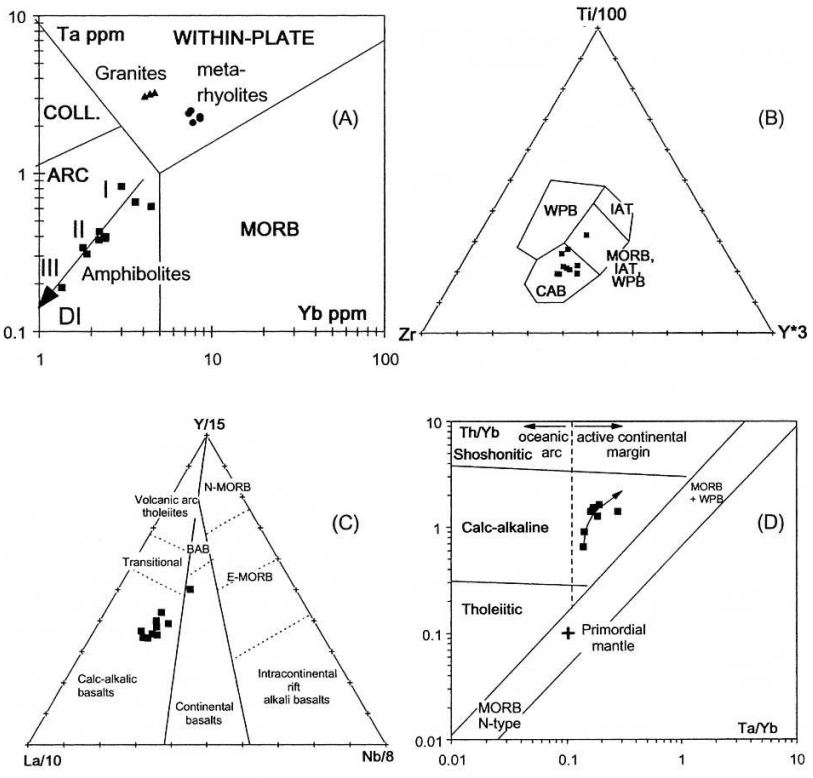

Fig. 10. (**a**) Yb versus Ta diagram discrimination diagram (Pearce 1982). The differentiation trend defined by the amphibolites is at the opposite of the metarhyolites. They belong to two different series. DI, differentiation. (**b**) Zr–Ti/100–Y*3 discrimination diagram (Pearce & Cann 1973). WPB, within-plate basalts; IAT, island arc tholeiites; MORB, mid-ocean ridge basalts; CAB, continental arc basalts. (**c**) La/10–Y/15–Nb/8 discrimination diagram (Cabanis & Lécolle 1989). BAB, back-arc basalts; N-MORB, normal mid-ocean ridge basalts; E-MORB, enriched mid-ocean ridge basalts. (**d**) Ta/Yb versus Th/Yb discrimination diagram (Pearce 1982). Abbreviations as (b) and (c).

shield (Caby & Andreopoulos-Renaud 1983), an event considered as intraplate. In both cases, this would require a younger amphibolite-facies metamorphism. Although such an event is not known in West Africa, it cannot be excluded. Another possibility would be to envisage a environment in which both the amphibolite and metarhyolite protoliths could be generated, as in the Cenozoic Western United States (i.e. Fitton *et al.* 1991). Other potentially similar magmatic occurrences, such as the Arefsa region (Briedj 1993) and in the SE of the Laouni terrane (Black *et al.* 1994) should be studied to constrain this palaeoenvironment. A main point brought by Tchilit is that pre-Pan-African non-granulitic terranes can be preserved in the Tuareg shield, which can throw some light on the very poorly known Palaeo- and Mesoproterzoic evolution of this region.

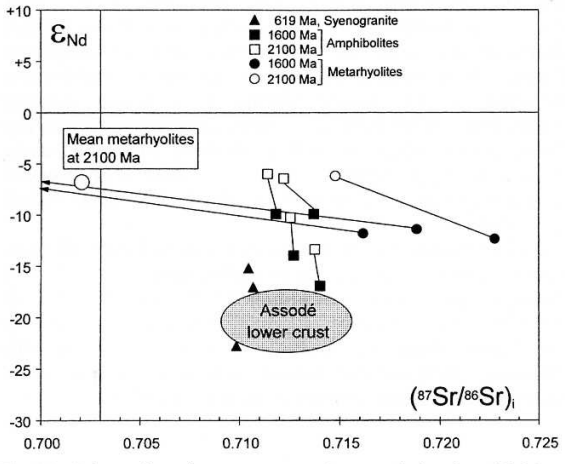

Fig. 11. Sr isotopic ratios versus ε_{Nd} values recalculated at 619 Ma for the syenogranite (age given by the Rb–Sr isochron) and in the 1600–2100 age interval for the amphibolites and the metarhyolites (the values at the two ages for each sample are linked by a line. The Assodé lower crust field is based on the Renatt anatectic granite from the Iko area (Liégeois *et al.* 1994) at 619 Ma.

Syenogranites. The three syenogranite spidergrams (Fig. 12c) are similar except sample BLN281 that has lower Hf, Zr, Ce and Ba. This sample has been taken from a small granitic outcrop surrounded by amphibolites and metarhyolites while the two others come from the main Tchilit massif. In this ORG-normalized spidergram, the distinctive character of the Tchilit syenogranite, compared to reference granites (Pearce *et al.* 1984), is the intermediate values of the less incompatible elements (Hf, Zr, Sm, Y, Yb) between the post-collisional Tibet granite and the alkaline Mull granite. This is in agreement with its late to post-kinematic character. Indeed, the Tuareg shield is characterized by a transition from calc-alkaline to alkaline at the end of the Pan-African (Liégeois & Black 1987; Azzouni-Sekkal & Boissonnas 1993). The REE (Fig. 12d) are characterized by steep LREE with La_N between 150 and 300, a rather large Eu anomaly and flat HREE at a normalized value around 20. These spectra are similar in shape to the Tchilit metarhyolites, although less enriched in all REE. These two magmatic events could represent two melting episodes of the same source. The isotopic initial values at 619 Ma of the syenogranite (Sr_i=0.710; ε_{Nd}= − 15 to − 23; Fig. 11)

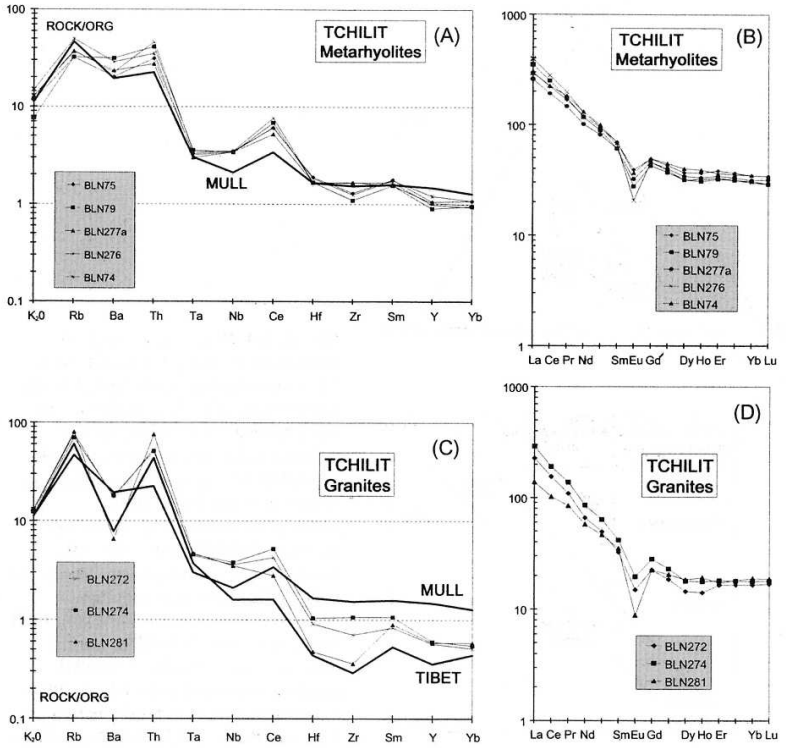

Fig. 12. (**a**) Spidergram normalized to ocean ridge granite (Pearce *et al.* 1984) of the metarhyolites and of a reference granite (alkaline Mull granite). (**b**) Rare earth elements patterns normalized to chrondrites of the metarhyolites from the Tchilit terrane. (**c**) Spidergram normalized to ocean ridge granite (Pearce *et al.* 1984) of the granite and of reference granites (collision-related Tibet granite and within-plate alkaline Mull granite). (**d**) Rare earth element patterns normalized to chrondrites of the granite from the Tchilit terrane.

allow that hypothesis if the source is a Rb-depleted lower crust. These values are also close to the Archaean lower crust of the adjacent Assodé Terrane (at 619 Ma, $Sr_i = 0.710$ and $\varepsilon_{Nd} = -20$ to -23) represented by the anatectic Renatt granite in the Iko area (Liégeois *et al.* 1994).

Conclusions

(1) The Tchilit block belongs to the Tuareg assembly of terranes (Black *et al.* 1994) in Aïr but, as no lithological correlations can be drawn with the adjacent terranes, it is considered as exotic. It does not represent a Pan-African rift within the Assodé terrane evolution as was previously envisaged in the field (Liégeois *et al.* 1994). Some other 'Pharusian basins' as in the Arefsa or in SE Laouni terranes could be equivalent.

(2) The Tchilit terrane is composed of amphibolites (meta-basalts to meta-andesites) and metarhyolites belonging to a Palaeoproterozoic orogeny not precisely defined (in the 2100–1600 Ma range), Neoproterozoic metasediments and late to post-kinematic syenogranites of late Pan-African age (619 ± 39 Ma).

(3) The two volcanic series have been affected by a mylonitic amphibolite-facies metamorphism (*c.* 700°C) during this Palaeoproterozoic orogeny and by a discrete greenschist-facies retrogression dated at 646 ± 6 Ma during the Pan-African orogeny.

(4) The amphibolite protoliths represent a low-K calc-alkaline series from a continental active margin; the rhyolites belong to an alkaline series, maybe emplaced in the same setting.

(5) An early Archaean lower crust as shown by the Sm–Nd systematics has contaminated both amphibolites and metarhyolites. This Archaean crust at depth is fundamentally different from the contemporaneous Birimian crust from the West African craton which is entirely juvenile (Abouchami *et al.* 1990; Ama Salah *et al.* 1996).

(6) The Pan-African effects on the Tchilit terrane are late, related to N–S dextral movements and comprise a granitic intrusion probably of lower crustal origin sharing geochemical characteristics with the Palaeoproterozoic metarhyolites. Finally, N–S dextral movements generated transpressive thrusting of the Assodé terrane onto Tchilit inducing greenschist metamorphism, mylonitization and folding. These events reflect an oblique docking of Tchilit along Assodé during a northern migration, which is the general direction of terrane movements in the Tuareg shield (Black *et al.* 1994).

(7) The existence of exotic terranes such as Tchilit, the only known Palaeoproterozoic non-granulitic terrane in the Tuareg shield, or Iskel, alone in recording the 870–850 Ma old orogeny (Caby *et al.* 1982; Fig. 1), demonstrate that the terranes of the Tuareg shield are likely to have travelled over long distances during the Pan-African cycle as in the case of the Mesozoic cordilleran terranes of western America.

We gratefully acknowledge the help of S. Mammadou, Secrétaire Général du Ministère des Mines et de l'Energie du Niger, for logistical support and facilities. The Ar–Ar work is part of a postdoctoral grant by the Belgian National Science Foundation (NFWO-FNRS) to A. Boven. We thank an anonymous reviewer for his constructive criticism of the manuscript.

References

ABOUCHAMI, W., BOHER, M., MICHARD, A. & ALBARÈDE, F. 1990. A major 2.1 Ga event of mafic magmatism in West Africa: an early stage of crustal accretion. *Journal of Geophysical Research,* **95, B11,** 17 605–17 629.

AMA SALAH, I., LIÉGEOIS, J.P. & POUCLET, A. 1996. Evolution d'un arc insulaire océanique birimien précoce au Liptako nigérien (Sirba), géologie, géochronologie et géochimie. *Journal of African Earth Sciences,* **22,** 235–254.

AZZOUNI-SEKKAL, A. & BOISSONNAS, J. 1993. Une province magmatique de transition du calco-alcalin à l'alcalin: les granitoïdes pan-africains à structures annulaires de la chaîne pharusienne du Hoggar (Algérie). *Bulletin de la Société Géologique de France,* **164,** 597–608.

BAKSI, A.K., ARCHIBALD, D.A. & FARRAR, E. 1996. Intercalibration of 40Ar/39Ar dating standards. *Chemical Geology,* **129,** 307–324.

BERTRAND, J.M.L., CABY, R., LANCELOT, J.R., MOUSSINE-POUCHKINE, A. & SAADALLAH, A. 1978. The late Pan-African intracontinental lineat fold belt of the eastern Hoggar (Central Sahara, Algeria): geology, structural development, U-Pb geochronology, tectonic implication for the Hoggar shield. *Precambrian Research,* **7,** 349–376.

BLACK, R. & LIÉGEOIS, J.P. 1993. Cratons, mobile belts, alkaline rocks and the continental lithospheric mantle: the Pan-African testimony. *Journal of the Geological Society, London,* **150,** 89–98.

——, JAUJOU, M. & PELLATON, C. 1967. *Notice explicative de la carte géologique de l'Aïr à l'échelle 1/500000. Direction Nationale des Mines et de la Géologie, Niger.*

——, LIÉGEOIS, J.P., LATOUCHE, L., CABY, R. & BERTRAND, J.M. 1994. Pan-African displaced terranes in the Tuareg shield (Central Sahara). *Geology,* **22,** 641–644.

BRIEDJ, M. 1993. *Etude géologique de la région de Tahifet (Hoggar central, Algérie). Implications géodynamiques.* Thèse Université Nancy I.

BRUGUIER, O., DADA, S. & LANCELOT, J.R. 1994. Early Archaean component (>3.5 Ga) within a 3.05 Ga orthogneiss from northern Nigeria: U-Pb zircon evidence. *Earth and Planetary Science Letters,* **125,** 89–103.

CABANIS, B. & LÉCOLLE, M. 1989. Le diagramme La/10-Y/15-Nb/8: un outil pour la discrimination des séries volcaniques et la mise en évidence des processus de mélange et/ou de contamination crustale. *Comtes Rendus de l'Académie des Sciences de Paris, Série II,* **309,** 2023–2029.

CABY, R. & ANDREOPOULOS-RENAUD, U. 1983. Age à 1800 Ma du magmatisme sub-alcalin associé aux métasédiments monocycliques dans la chaîne pan-africaine du Sahara central. *Journal of African Earth Sciences,* **1,** 193–197.

——, —— & GRAVELLE, M. 1982. Cadre géologique et géochronologique U/Pb sur zircon des batholites précoces dans le segment pan-africain du Hoggar central (Algérie). *Bulletin de la Société Géologique de France,* **24,** 677–684.

FITTON, J.G., JAMES, D. & LEEMAN, W.P. 1991. Basic magmatism associated with late Cenozoic extension in the Western United States: compositional variations in space and time. *Journal of the Geophysical Research,* **96,** 13 693–13 711.

HARRISON, T.M. 1981. Diffusion of ^{40}Ar in Hornblende. *Contributions to Mineralogy and Petrology,* **78,** 324–331.

HESS, J.C. & LIPPOLT, H.J. 1994. Compilations of K-Ar measurements on HD-B1 standard biotite 1994 status report. *In*: G.S. ODIN (ed.) Phanerozoic Time Scale. Bulletin de Liaison et d'Information, IUGS Subcommission of Geochronology, **12,** 19–23.

HOLLAND, T.J.B. & BLUNDY, J. 1994. Non-ideal interactions in calcic amphiboles and their bearing on amphibole-plagioclase thermometry. *Contribution to Mineralogy and Petrology,* **116,** 433–447.

KELLEY, S.P. & TURNER, G. 1991. Laser probe ^{40}Ar-^{39}Ar measurements of loss profiles within individual hornblende grains from the Giants Range Granite, northern Minnesota, USA. *Earth and Planetary Science Letters,* **107,** 634–648.

LATOUCHE, L. & VIDAL, P. 1974. Géochronologie du Précambrien de la région des Gour Oumelalen (N.E. de l'Ahaggar, Algérie); un exemple de mobilisation du strontium radiogénique. *Bulletin de la Société Géologique de France,* **16,** 195–203.

LIÉGEOIS, J.P. & BLACK, R. 1987. Alkaline magmatism subsequent to collision in the Pan-african belt of the Adrar des Iforas (Mali). *In*: FITTON, J.G. & UPTON, B.J.G. (eds) *Alkaline Igneous Rocks.* Geological Society, London, Special Publications, **30,** 381–401.

——, ——, NAVEZ, J. & LATOUCHE, L. 1994. Early and late Pan-African orogenies in the Aïr assembly of terranes (Tuareg shield, Niger). *Precambrian Research,* **67,** 59–88.

——, CLAESSENS, W., CAMARA, D. & KLERKX, J. 1991. Short-lived Eburnian orogeny in southern Mali. Geology, tectonics, U-Pb and Rb-Sr geochronology. *Precambrian Research,* **50,** 111–136.

MIYASHIRO, A. 1974. Volcanic rocks series in island arcs and active continental margins. *American Journal of Science,* **274,** 321–355.

MOREAU, C., DEMAIFFE, D., BELLION, Y. & BOULLIER, A.M. 1994. A tectonic model for the location of Paleozoic ring-complexes in Aïr (Niger, West Africa). *Tectonophysics,* **234,** 129–146.

NAVEZ, J. 1983. Détermination de 11 éléments en traces dans les roches silicatées par spectrométrie d'émission dans un plasma à couplage inductif. *Rapport Annuel du Département de Géologie et Minéralogie 1981–1982.* Musée Royal de l'Afrique Centrale, Tervuren, Belgique, 115–118.

—— 1995. Détermination d'éléments en traces dans les roches silicatées par ICP-MS. *Rapport Annuel du Département de Géologie et Minéralogie 1993–1994.* Musée Royal de l'Afrique Centrale, Tervuren, Belgique, 139–147.

NORRISH, K. & HUTTON, J.T. 1969. An accurate X-ray spectrographic method for the analysis of a wide range of geological samples. *Geochimica et Cosmochimica Acta,* **33,** 431–453.

PEARCE, J. 1982. Role of the sub-continental lithosphere in magma genesis at active continental margins. *In*: HAWKESWORTH, C.J. & NORRY, M.J. (eds) *Continental basalts and mantle xenoliths.* Shiva Geology Series, Nantwich, 230–249.

—— & CANN, J.R. 1973. Tectonic setting of basic volcanic rocks determined using trace element analyses. *Earth and Planetary Science Letters,* **19,** 290–300.

——, HARRIS, N.B.W. & TINDLE, A.G. 1984. Trace element discrimination diagrams for the tectonic interpretation of granitic rocks. *Journal of Petrology,* **25,** 956–983.

STEIGER, R.H. & JÄGER, E. 1977. Subcommission on geochronology: convention on the use of decay constants in geo- and cosmochronology. *Earth and Planetary Science Letters,* **36,** 359–362.

SUN, S.S. 1980. Lead isotopic study of young volcanic rocks from mid-ocean ridges, ocean islands and islands arcs. *Philosophical Transactions of the Royal Society of London,* **A297,** 409–445.

VILLA, I.M., GROBETY, B., KELLEY, S.P., TRIGILA, R. & WIELER, R. 1996. Assessing Ar transport paths and mechanisms in the McClure Mountains hornblende. *Contributions to Mineralogy and Petrology,* **126,** 67–80.

WARTHO, J.A. 1995. Apparent argon diffusive loss 40Ar/39Ar age spectra in amphiboles. *Earth and Planetary Science Letters,* **134,** 393–407.

WILLIAMSON, J.H. 1968. Least square fitting of a straight line. *Canadian Journal of Physics,* **46,** 1845–1847.

Received 10 May 1997; revised typescript accepted 22 September 1998.
Scientific editing by Hugh Rollinson.